Volume 15
Number 2
14 January 2024
Pages 401–782

Chemical Science

rsc.li/chemical-science

ISSN 2041-6539

ROYAL SOCIETY OF CHEMISTRY

EDGE ARTICLE

Anne Staubitz *et al.*

Boosting quantum yields and circularly polarized luminescence of penta- and hexahelicenes by doping with two BN-groups

Chemical Science

ROYAL SOCIETY OF CHEMISTRY

EDGE ARTICLE

View Article Online
View Journal | View Issue

Cite this: *Chem. Sci.*, 2024, **15**, 466

All publication charges for this article have been paid for by the Royal Society of Chemistry

Boosting quantum yields and circularly polarized luminescence of penta- and hexahelicenes by doping with two BN-groups†

Yannik Appiarius, [ab] Sandra Míguez-Lago, [c] Pim Puylaert, [d] Noah Wolf, [a] Sourabh Kumar, [e] Martin Molkenthin,[a] Delia Miguel, [f] Tim Neudecker, [beg] Michal Juríček, [h] Araceli G. Campaña [c] and Anne Staubitz *[ab]

Received 26th May 2023
Accepted 23rd October 2023

DOI: 10.1039/d3sc02685j

rsc.li/chemical-science

The incorporation of boron–nitrogen (BN) units into polycyclic aromatic hydrocarbons (PAHs) as an isoelectronic replacement of two carbon atoms can significantly improve their optical properties, while the geometries are mostly retained. We report the first non-π-extended penta- and hexahelicenes comprising two aromatic 1,2-azaborinine rings. Comparing them with their all-carbon analogs regarding structural, spectral and (chir)optical properties allowed us to quantify the impact of the heteroatoms. In particular, BN-hexahelicene **BN[6]** exhibited a crystal structure congruent with its analog **CC[6]**, but displayed a fivefold higher fluorescence quantum yield (φ_{fl} = 0.17) and an outstanding luminescence dissymmetry factor ($|g_{lum}| = 1.33 \times 10^{-2}$). Such an unusual magnification of both properties at the same time makes BN-helicenes suitable candidates as circularly polarized luminescence emitters for applications in materials science.

Introduction

Circularly polarized luminescence (CPL) is the differential emission of left- (I_L) and right-handed (I_R) circularly polarized light by chiral luminophores.[1] Recently, CPL-active materials have demonstrated their immense application potential for optoelectronics,[2–4] 3D displays,[5,6] switches for data storage,[7,8] spintronics[9,10] or chiral sensors.[11,12]

Small organic molecules are particularly suitable as CPL emitters due to their structural modifiability.[13] It allows the tuning of crucial optical properties like molar absorptivities (ε), fluorescence quantum yields (φ_{fl}) or emission dissymmetry factors ($g_{lum} = 2 \times (I_L - I_R)/(I_L + I_R)$), quantifying the degree of polarization in the emission. Moreover, structure-related parameters like configurational[14] and thermal[15] stabilities towards decomposition are tunable, which is of high relevance for the processing into functional materials.

Among the various classes of chiral, π-conjugated molecules, helicenes are well-known for their strong optical rotation and electronic circular dichroism (ECD).[16] Carbohelicenes are chiral, screw-shaped polycyclic aromatic hydrocarbons (PAHs) with $n \geq 5$ *ortho*-fused benzenoid rings.[17] Research studies have especially focused on derivatives of pentahelicene and hexahelicene because they allow chiral resolution at ambient conditions[18] and gram-scale preparation by various synthetic approaches.[19]

For assessing the suitability of helicenes as CPL-emitting molecules, key prerequisites are high $|g_{lum}|$ values, but also elevated ε and φ_{fl}. To combine these parameters into one, the CPL brightness factor $B_{CPL} = 0.5 \times \varepsilon \times \varphi_{fl} \times |g_{lum}|$ has been introduced,[20] allowing to compare the suitability of such luminophores for potential applications. Planar PAHs typically display high φ_{fl} values due to electronically allowed π–π* transitions, but the distorted π-planes of helicenes induce a significant decrease (φ_{fl} = 0.04 for both penta- and hexahelicene). This is a result of accelerated intersystem crossing, leading to non-emissive triplet states.[21] Furthermore, the dissymmetry factors of carbohelicenes are almost exclusively below 10^{-2} ($|g_{lum}| = 2.7 \times 10^{-3}$ for penta- and 9×10^{-4} for

[a]*University of Bremen, Institute for Organic and Analytical Chemistry, 28359 Bremen, Germany. E-mail: staubitz@uni-bremen.de*
[b]*University of Bremen, MAPEX Center for Materials and Processes, 28359 Bremen, Germany*
[c]*University of Granada, Department of Organic Chemistry, Unidad de Excelencia de Química, 18071 Granada, Spain*
[d]*University of Bremen, Institute for Inorganic Chemistry and Crystallography, 28359 Bremen, Germany*
[e]*University of Bremen, Institute for Physical and Theoretical Chemistry, 28359 Bremen, Germany*
[f]*University of Granada, Department of Physical Chemistry, Unidad de Excelencia de Química, 18071 Granada, Spain*
[g]*University of Bremen, Bremen Center for Computational Materials Science, 28359 Bremen, Germany*
[h]*University of Zurich, Department of Chemistry, 8057 Zurich, Switzerland*

† Electronic supplementary information (ESI) available: Experimental procedures, single crystal data, HPLC chromatograms, kinetic data, photophysical data, NMR spectra and DFT calculations. CCDC 2192803, 2192802, 2192799, 2192801, 2212001 and 2212000. For ESI and crystallographic data in CIF or other electronic format see DOI: https://doi.org/10.1039/d3sc02685j

hexahelicene).[22,23] Consequently, pristine carbohelicenes (B_{CPL} < 2 M^{-1} cm^{-1}) are barely useful as CPL emitters.[24]

Incorporating main group elements like nitrogen,[25–27] oxygen,[28,29] silicon[30,31] or combinations of these (*e.g.* B–O)[32] in PAHs in general can modulate the optical properties significantly. However, this also perturbs the molecular architecture and the estimation of structural and electronic influences isolated from each other is complicated.[33]

Therefore, the doping with neighboring boron–nitrogen (BN) units has emerged as a popular strategy especially for planar PAHs,[35–38] as it provides isoelectronic and isostructural BN-PAHs. In such compounds, the disparities in properties are almost exclusively caused by altered electronegativities of the heteroatoms,[39] facilitating the comparison with the parent, all-carbon CC-PAHs.[40–42]

Unfortunately, reports of helical BN-derivatives have remained scarce,[43–47] which especially applies to helicenes with B=N groups in the aromatic backbone.[48,49] Moreover, experimental studies that compare BN-helicenes with their all-carbon counterparts are rare. To our knowledge, the work from Nowak-Król and Ingleson describes the only non-π-extended B=N-helicenes so far (Fig. 1, top right).[50] Besides a small structural impact, the most distinctive effect was an amplification of the radiative decay (φ_{fl} = 0.30 for the (mono)BN-pentahelicene, φ_{fl} = 0.21 for the BN-hexahelicene), compared to the all-carbon congeners, which were calculated but not synthesized. Nevertheless, this suggests the great potential of this compound class.

Herein, we present the first non-π-extended penta- and hexahelicenes **BN[5]** and **BN[6]**, respectively, comprising two aromatic boron–nitrogen-containing rings (Fig. 1, bottom). A multi-dimensional comparison with their all-carbon analogs **CC[5]** and **CC[6]** allowed us to gauge the exact influence of the BN-substitution on structural and (chir)optical properties. Most strikingly, the BN-substitution led to an outstanding CPL brightness of **BN[6]** (B_{CPL} = 59 M^{-1} cm^{-1}) while leaving the geometrical structure almost unaffected.

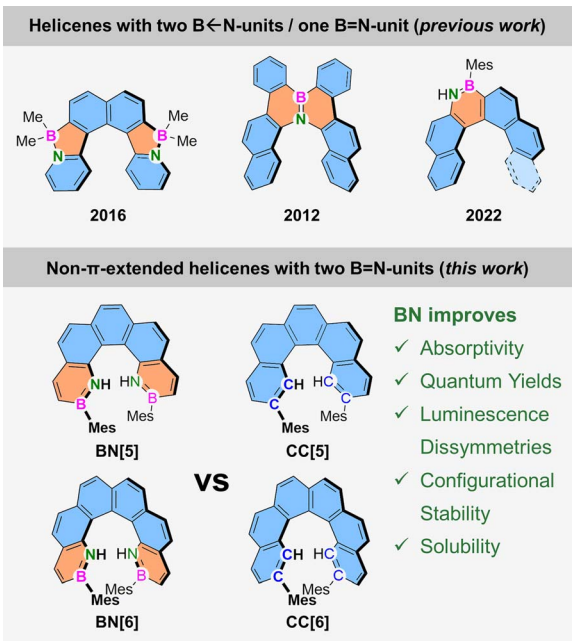

Fig. 1 Top: previously reported BN-penta- and hexahelicenes. Bottom: structures studied in this work and the demonstrated benefits of such a twofold BN-substitution.[34]

Results and discussion

Syntheses

BN-helicenes **BN[5]** and **BN[6]** were synthesized *via* transition-metal-catalyzed electrophilic cyclizations of (bis)ethynylarene precursors. These mild conditions[51–53] were chosen to ensure the integrity of the moderately acidic, *N*-deprotected 1,2-azaborinine building blocks.

Initially, electrophilic benzene- **1** and naphthalene precursors **2**, equipped with two (trimethylsilyl)ethynyl substituents, were synthesized (Scheme 1).[52] Subsequent Suzuki–Miyaura cross-coupling reactions with nucleophilic mesitylazaborinine **3** (ref. 54) gave TMS-alkynes **4** and **5** in yields of 72% and 75%, respectively. Under basic reaction conditions, deprotected alkynes **6** and **7** were obtained quantitatively.

Our previous study of planar BN-PAHs[55] showed that six-membered rings are formed almost exclusively when reacting the deprotected arylalkynes with $PtCl_2$ at 100 °C. Transferring these conditions to BN-helicenes, however, significantly favored the competing 5-*exo-dig* pathway, leading to dibenzofulvene-like side-products in conversions of more than 40%. Therefore, we investigated different catalytic systems based on Pt(II), Au(I), Au(III) and Ru(II) (see ESI, Tables S1 and S2†).

In the case of **BN[5]**, the reaction of phenylalkyne **6** with $AuCl_3$ at 100 °C for 24 h provided the highest conversion with less than 5% *endo*/*exo*-side product **8** (see ESI, Table S1†). Derivatization of the latter with piperidine[56] and chromatographic separation of the resulting Michael-type adduct eventually allowed the isolation of **BN[5]** in 54% yield.

On the other hand, the cyclization of naphthylalkyne **7** to **BN[6]** was achieved using $[(p\text{-cymene})RuCl_2]_2$ and $AgSbF_6$. Among all catalytic systems tested, this was the only one that favored the formation of two six-membered rings (*ca.* 80% of *endo*/*endo*) (see ESI, Table S2†). We assume that the reaction with Ru(II) preferably proceeds *via* the η^1-vinylidene intermediate, assisting the nucleophilic attack at the terminal alkyne carbon.[57] After heating **7** and the catalysts to 170 °C for 1 h in mesitylene and purification as for **BN[5]**, **BN[6]** was obtained in a yield of 11% (Scheme 1). In contrast to the Ru(II) catalyst, the use of $AuBrPPh_3$ and $AgSbF_6$ allowed to selectively synthesize and isolate *endo*/*exo*-derivative **9** (see ESI, Section 2.28†).

For the syntheses of **CC[5]** and **CC[6]** (phenylethenyl)phenanthrene **10** and bis(phenylethenyl)naphthalene **11** were prepared in total yields of 52% and 18%, respectively. Mallory photocyclization reactions using UV irradiation at λ = 365 nm in the presence of iodine and propylene oxide gave dibromopenta- **12** and dibromohexahelicene **13**. Subsequently, mesityl substituents were installed at positions 2,13 and 2,15, respectively, *via* Kumada cross-coupling reactions with mesitylmagnesium bromide. Eventually, racemic mixtures of **CC[5]**

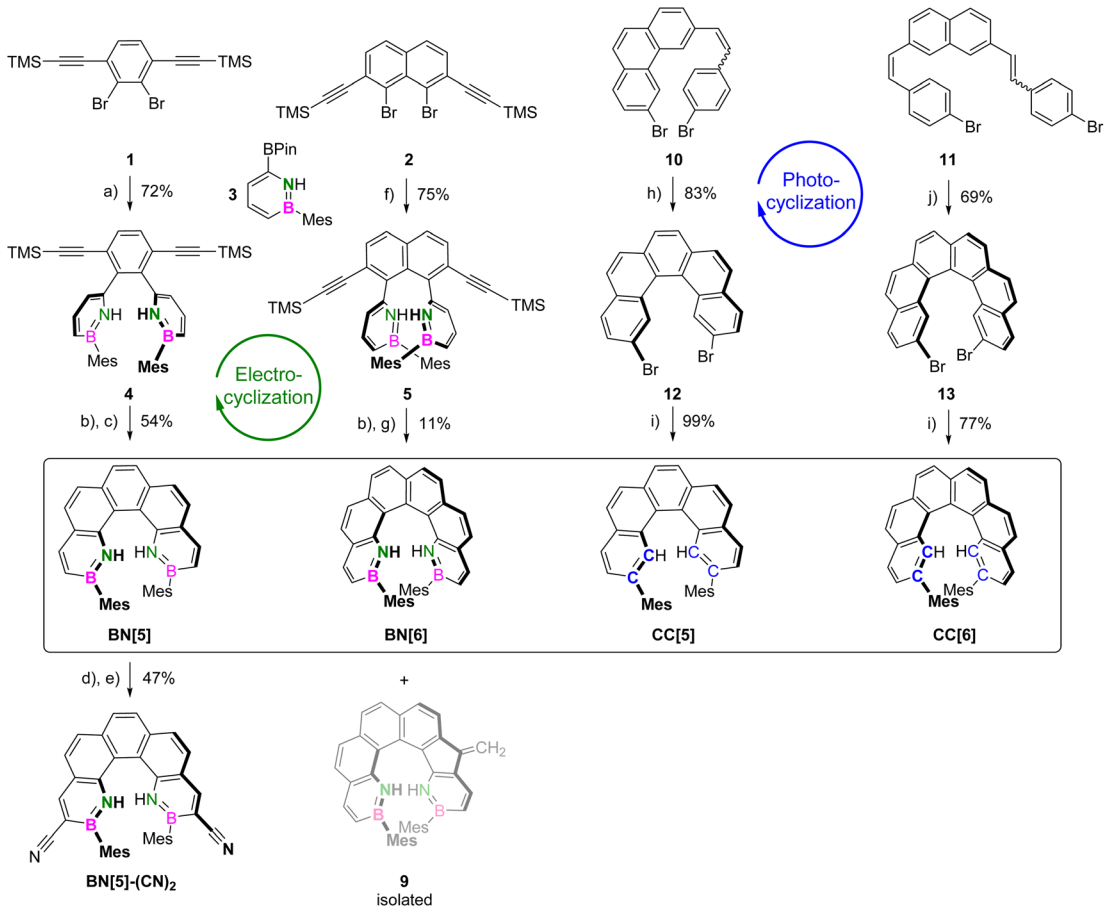

Scheme 1 Syntheses of BN- and CC-helicenes. Reagents and conditions: (a) **3** (4.0 equiv.), potassium phosphate (3.0 equiv.), $[Pd(dppf)Cl_2]$ (5 mol%), methyl *tert*-butyl ether (MTBE), water, 90 °C, 2 d; (b) KOH (2.0 equiv.), MeOH, Et_2O, 25 °C, 3 h; (c) 1. $AuCl_3$ (30 mol%), mesitylene, 100 °C, 24 h; 2. Piperidine, acetonitrile, 25 °C, 1 h; (d) Bromine (2.2 equiv.), DCM, 0 °C, 2 h; (e) CuCN (10 equiv.), DMF, 170 °C, 19 h; (f) **3** (4.0 equiv.), potassium phosphate (3.0 equiv.), $[Pd_2(dba)_3]$ (5 mol%), SPhos (10 mol%), THF, water, 60 °C, 17 h; g) 1. $[(p\text{-cymene})RuCl_2]_2$ (30 mol%), $AgSbF_6$ (30 mol%), mesitylene, 170 °C, 1 h; 2. Piperidine, acetonitrile, 25 °C, 1 h; (h) Iodine (1.1 equiv.), propylene oxide (500 equiv.), toluene, 365 nm LED, 25 °C, 30 min; (i) MesMgBr (3.0 equiv.), $[Pd(dppf)Cl_2]$ (5 mol%), 1,4-dioxane, 95 °C, 3 d; (j) Iodine (2.2 equiv.), propylene oxide (500 equiv.), toluene, 365 nm LED, 25 °C, 3 h.

and **CC[6]** were obtained in yields of 82% and 53% over the last two steps (Scheme 1).

Introducing functional groups onto a pre-existing helicene scaffold by electrophilic aromatic substitution is highly desirable but often demanding. In a 1,2-azaborinine, the uneven charge distribution renders all carbon atoms distinct in reactivity.[58] In particular, the selective electrophilic bromination at the α-carbon adjacent to boron has been shown to be a viable starting point for post-functionalizations.[59–61] This methodology allowed us to selectively synthesize 3,12-dibrominated **BN[5]-Br$_2$** in 75% yield by the reaction of **BN[5]** with 2.2 equiv. of bromine. Subsequently, the conversion with an excess of copper(I) cyanide under Rosenmund–von Braun conditions gave **BN[5]-(CN)$_2$** in a yield of 62% (Scheme 1). In contrast, the reaction of **CC[5]** with bromine gave the C5,C6-dibrominated adduct.[62] Upon heating it to 130 °C, rearomatization occurred and a mixture of reactant and the C5-brominated derivative was obtained. This highlights the superior selectivity of BN-PAHs in such a reaction (see ESI, Section 2.29†).

Structural analysis

Single crystals of the racemic target compounds suitable for X-ray diffraction analysis were obtained by vapor diffusion of acetonitrile, methanol, cyclohexane or *n*-hexane into DCM solutions of the helicenes.

Comparing the bond lengths within the terminal rings (B–N: 1.426 ± 0.003 Å, C1–C2: 1.385 ± 0.003 Å, $\Delta d \approx 3\%$) showed the expected, relatively small geometric effect of the BN-substitution. Moreover, the C–C bond lengths within outer (1.34–1.38 Å) and inner helices (1.43–1.46 Å) remained almost identical, confirming the high two-dimensional isostructuralism of carbo- and BN-helicenes.[63] On the other hand, the effect of BN on the spatial configurations of the pentahelicenes was remarkable (Fig. 2). Compared to **CC[5]** ($\varphi = 52.4°$), the torsion angle (φ) between the terminal rings (*A*) was only $\varphi = 42.8°$ in **BN[5]**, pointing at attracting interactions involving the NH units in close proximity (d (NH···N) = 2.35 Å).

This also has implications on the molecular arrangements. While the packing structures of both compounds consist of

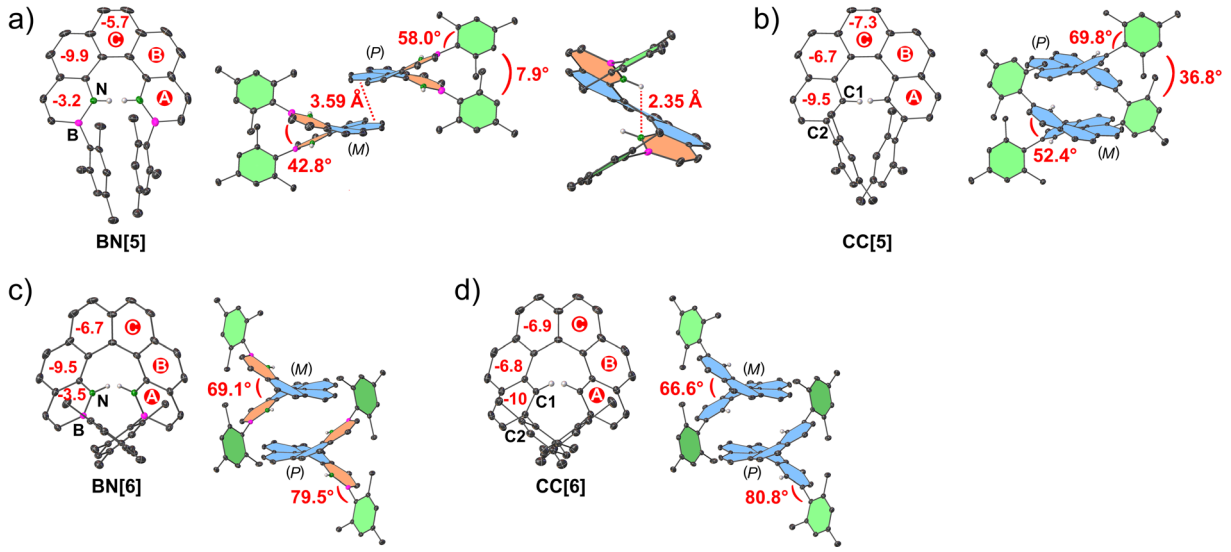

Fig. 2 Solid-state structures as obtained from X-ray diffraction analysis. Thermal ellipsoids are shown at a 50% probability level. Hydrogen atoms (except for N–H and C1–H) are omitted for clarity. NICS(0) values for the individual rings were calculated at the MP2 (ref. 64)/cc-pVDZ[65] level of theory, as implemented in the Q-Chem 6.0 program package.[66] C_2 symmetry was assumed so that angles and distances are given as average values of both sides of the molecules.

opposite pairs of (*P*)- and (*M*)-enantiomers, there is a significant overlap of the helicene scaffolds ($d = 3.59$ Å between rings C) in a **BN[5]** crystal, hinting at the presence of π–π-interactions. Furthermore, the mesityl groups of each molecule are oriented almost parallelly ($\varphi = 7.9°$), which leads to a highly ordered packing arrangement. In **CC[5]**, rings A and B of opposite molecules are arranged co-planarly but displaced. Also, the interplanar angle between the mesityl groups is larger ($\varphi = 36.8°$). The structural parameters of **BN[5]-(CN)$_2$** were mostly comparable with **BN[5]** (see ESI, Section 3.3†).

Both hexahelicenes exhibit much more similar metrics ($\varphi = 69.1°$ for **BN[6]**, $\varphi = 66.6°$ for **CC[6]** between rings A), identical packing modes (see ESI, Fig. S10 and S14†) and very similar unit-cell parameters. The absence of additional dipolar interactions in **BN[6]** indicates that for hexahelicenes, the distant BN-units do not play a structure-determining role.

Besides the high planarity of the 1,2-azaborinine rings (averaged $\varphi = 2.6°$ within rings A), aromaticity was clearly confirmed by nucleus-independent chemical shift (NICS) calculations (NICS(0) < −3 ppm, Fig. 2).[67]

Optical spectroscopy

Absorption and fluorescence spectra as well as φ_{fl} and fluorescence lifetimes (τ_{fl}) of the investigated helicenes were acquired in DCM solutions (Table 1).

BN[5], **CC[5]**, **BN[6]** and **CC[6]** revealed comparable absorption maxima ($\lambda_{abs} = 266$–283 nm) with decent molar extinction coefficients ($\varepsilon = 3.4$–5.2×10^4 M^{-1} cm^{-1} see ESI, Fig. S18–S22†). The absorption bands of both hexahelicenes closely resembled each other with small bathochromic shifts of **BN[6]** ($\Delta\lambda_{abs} \approx$ 10–15 nm, Fig. 3b). This suggests similar energy orderings of the differently polarized dipole transition moments.[68] Most remarkably, the BN-moieties induced a substantial intensification of the least energetic ^1L_b band, which is associated with fluorescence[69] (**BN[6]**: $\varepsilon = 3300$ M^{-1} cm^{-1} at 424 nm, **CC[6]**: $\varepsilon = 200$ M^{-1} cm^{-1} at 414 nm).[70,71] With respect to the pentahelicenes, the absorption spectra were more different in shape but both revealed shoulder bands at $\lambda_{abs} \approx 400$ nm. The ε value of the lowest-energy transition of **BN[5]** was intensified by about an order of magnitude as well (Fig. 3a). This is a typical effect of BN-doping, rendering the symmetry-forbidden $S_0 \rightarrow S_1$ transition of all-carbon aromatics partially allowed.[72]

The fluorescence spectra of all five compounds consisted of at least three distinct vibronic bands, and the Stokes shifts, if determinable, were small (≈600 cm^{-1}, Fig. 3). Compared to the very similar emission bands of the pentahelicenes ($\lambda_{fl} \approx$ 410 nm, $\Delta\lambda_{fl} = 2$ nm for the 0–0 bands), the difference between the hexahelicenes was slightly more pronounced ($\lambda_{fl} = 434$ nm for **BN[6]**, $\lambda_{fl} = 423$ nm for **CC[6]**).

Moreover, the bathochromic effect of a twofold BN-substitution was identified by comparison with the reported (mono)BN-hexahelicene (Fig. 1, top right, $\lambda_{abs} = 397$ nm, $\lambda_{fl} =$ 419 nm).[50] In terms of fluorescence quantum yields, the BN-helicenes were substantially brighter ($\varphi_{fl} = 0.10$ for **BN[5]**, $\varphi_{fl} = 0.17$ for **BN[6]**) than the sparsely emissive carbohelicenes ($\varphi_{fl} = 0.04$ for **CC[5]**, $\varphi_{fl} = 0.03$ for **CC[6]**). Furthermore, the intensity averaged τ_{fl} of the heterohelicenes were comparably smaller than those of the studied carbohelicenes. While the difference was just 20% for the hexahelicenes, the lifetime of **BN[5]** ($\tau_{fl} =$ 4.7 ns) was halved compared to **CC[5]** ($\tau_{fl} = 9.7$ ns). The increase of φ with a concomitant decrease of τ_{fl} for BN-helicenes can be rationalized with a larger emissive rate of these fluorophores compared to the all-carbon analogs. The influence of the mesityl-substitution on the optical features of the parent carbohelicenes (*cf.* hexahelicene: $\lambda_{abs} = 410$ nm, $\lambda_{fl} = 420$ nm, $\varphi_{fl} =$ 0.03, $\tau_{fl} = 8.4$ ns)[76] was negligible, emphasizing that the

Table 1 Experimental, photophysical properties of the investigated helicenes and calculated oscillator strengths f for the lowest-energy transitions

Compound	λ_{abs}[a,b] [nm] ($10^{-3} \times \varepsilon$ [M^{-1} cm^{-1}])	λ_{fl}[a,b,c] [nm]	φ_{fl}[a]	Stokes shift [cm^{-1}]	τ_{fl}[a] [ns]	f[f] (λ [nm])
BN[5]	**283** (48.2), 363 (14.7), 383 (12.6)	407, **428**	0.10	[d]	4.7	0.1599 (370)
CC[5]	**275** (34.2), 308 (27.0), 336 (14.8), 375 (1.0)	409, **425**	0.04	[d]	9.7[e]	0.0010 (372)
BN[6]	**280** (52.2), 342 (26.3), 401 (3.1), 424 (3.3)	**434**, 459	0.17	540	7.1[e]	0.0418 (400)
CC[6]	**266** (44.7), 318 (19.1), 390 (0.3), 414 (0.2)	**423**, 444	0.03	510	8.7[e]	0.0027 (387)
BN[5]-$(CN)_2$	**313** (28.0), 390 (14.9), 413 (16.6)	**424**, 446	0.25	630	3.5	0.0053 (415)

[a] Measurements performed in DCM solutions at $c = 2.4 \times 10^{-5}$ to 4.0×10^{-5} M. [b] Bold values represent intensity maxima. [c] LED, $\lambda_{ex} = 370$ nm (BN-helicenes), 300 nm (carbohelicenes). [d] Not determinable because the 0–0 transitions were present as shoulder bands ($\lambda_{abs} \approx 400$ nm). [e] Intensity averaged values because fluorescence decay consisted of more than one species (see ESI, Section 5.3 for more details). [f] TD-DFT at the B3LYP[73–75]/cc-pVDZ[65] level of theory.

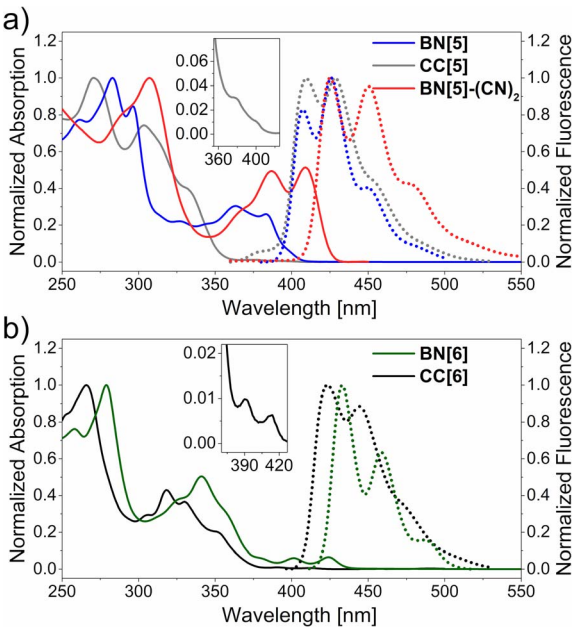

Fig. 3 Normalized absorption (continuous lines) and fluorescence (dotted lines) spectra of pentahelicenes (a) and hexahelicenes (b) in DCM ($c = 2.4 \times 10^{-5}$ to 4.0×10^{-5} M). Insets show the lowest-energy absorption (shoulder) bands of the carbohelicenes.

enhancement of the photophysical properties by the BN-unit should not be limited to this particular substitution pattern.

We further investigated the structural and electronic properties of the helicenes by time-dependent density functional theory (TD-DFT) calculations at the B3LYP[73–75]/cc-pVDZ[65] level of theory, as implemented in the Q-Chem 6.0 (ref. 66) and Gaussian 09, Rev. B.01 (ref. 77) program packages. For all helicenes, the emissive S_1 states[78] mostly consisted of highest occupied (HONTO) and lowest unoccupied (LUNTO) natural transition orbitals (NTOs). Moreover, the carbohelicenes revealed increased contributions of HONTO−1 and LUNTO+1 (see ESI, Section 7.4, Fig. S31†). All NTOs were delocalized over the PAH scaffolds with little to no involvement of the mesityl-groups due to their perpendicular orientations. Most noticeably, BN-substitution induced a symmetry break of the NTOs of **BN[5]** (C_s for HONTO, C_2 for LUNTO, both are C_2 symmetric for **CC[5]**). This feature is the cause of the higher φ_{fl} of the BN-helicenes, because the associated transition is rendered symmetry-allowed. Therefore, the related oscillator strength of **BN[5]** ($f = 0.1599$) was increased by more than two orders of magnitude compared to **CC[5]** ($f = 0.0010$). Despite the almost identically shaped NTOs of **BN[6]** and **CC[6]**, the BN-helicene still revealed a tenfold increase of f. Overall, these results rationalize the experimental increase of ε in the low-energy regions.

The change of the optical properties of **BN[5]** upon installation of cyano-substituents was remarkable and higher than for similarly functionalized carbohelicenes:[79] **BN[5]-$(CN)_2$** not only revealed an intensification and a bathochromic shift of the 0–0 absorption band ($\Delta\lambda_{abs} = 30$ nm), but was also the most emissive compound ($\varphi_{fl} = 0.25$). In combination with the short lifetime ($\tau_{fl} = 3.5$ ns), this indicates a particularly high fluorescence emission rate.

Chiral resolution & kinetics of racemization

The targeted helicenes were resolved into their enantiomers by high-performance liquid chromatography (HPLC), employing a chiral stationary phase (CSP). From a practical perspective, the pentahelicenes revealed a better resolution than the hexahelicenes with baseline-separated peaks (see ESI, Fig. S15 for chromatograms†). While **CC[6]** could not be resolved as a result of its low polarity concomitant with a poor solubility, **BN[5]** and **BN[6]** (enantiomeric excess ee = 99% for both) as well as **BN[5]-$(CN)_2$** (ee = 94%) and **CC[5]** (ee = 70%) were collected in their highly enantiomerically enriched forms.

This enabled the determination of the half-lives ($t_{1/2rac}$) and activation parameters of enantiomerization. For that purpose, each enantioenriched pentahelicene was subjected to time-course ECD measurements at 50, 60 and 70 °C. **BN[5]** showed a significantly lower racemization rate ($t_{1/2rac} \approx 80$ min at 60 °C) than **CC[5]** ($t_{1/2rac} \approx 20$ min). This translated into a Gibbs activation energy $\Delta G^{\ddagger}$ (25 °C) of 25.7 kcal mol^{-1} for **BN[5]**, which was higher by more than 1 kcal mol^{-1} compared to **CC[5]** (24.3 kcal mol^{-1}, Table 2, for Eyring plots and calculations see ESI, Section 4.2†). Despite the bulkiness of the mesityl groups, the 2,13 disubstitution had a comparably small effect on the configurational stability ($\Delta G^{\ddagger}$ (25 °C) = 24.1 kcal mol^{-1} for

Table 2 Kinetics of racemization and chiroptical properties obtained from ECD and CPL measurements

	Kinetics[b]		ECD[a]			CPL[a]		
Compound	$t_{1/2rac}$ [min]	$\Delta G^{\ddagger}$ (25 °C) [kcal mol^{-1}]	$\lambda_{max}{}^{e,f}$ [nm]	$\Delta\varepsilon$ [M^{-1} cm^{-1}] (λ_{max} [nm])	$10^3 \times \lvert g_{abs}\rvert^{g}$	$\lambda_{max}{}^{e,h}$ [nm]	$10^3 \times \lvert g_{lum}\rvert^{i}$	$B_{CPL}{}^{j}$ [M^{-1} cm^{-1}]
BN[5]	77.6	25.7	**304** (−), 373 (+), 393 (+)	276 (304), 111 (393)	9.9	423, **444**	4.2	10.1
CC[5]	21.1	24.3	276 (−), **319** (+), 337 (+), 399 (−)	152 (319), 82 (337)	6.0	**408**, 429	4.4	3.0
BN[6]	*c*		**285** (−), 344 (+), 409 (+), 431 (+)	151 (285), 28 (431)	10.8	**432**, 459	13.3	59.0
CC[6]	*d*		*d*			*d*		
BN[5]-(CN)$_2$	50.3	25.2	291 (+), **313** (−), 389 (+), 412 (+)	187 (313), 127 (412)	8.0	429	5.1	17.8

[a] Chiroptical measurements performed in DCM solutions at $c = 1.3 \times 10^{-5}$ to 4.0×10^{-5} M. [b] By time-course ECD measurements in *n*-heptane. $t_{1/2rac}$ at 60 °C. [c] Not measurable due to decomposition before reaching a temperature sufficient for racemization. [d] Not determined because chiral resolution by (CSP)-HPLC was unsuccessful. [e] Bold values represent intensity maxima. [f] Signs for (*P*)-enantiomers. (−) = negative CE, (+) = positive CE. [g] $g_{abs} = \Delta\varepsilon/\varepsilon$ for the lowest energetic CE. [h] $\lambda_{ex} = 370$ nm (BN-helicenes), $\lambda_{ex} = 300$ nm (carbohelicenes). [i] $g_{lum} = 2 \times (I_L - I_R)/(I_L + I_R)$. [j] $B_{CPL} = 0.5 \times \varepsilon \times \varphi_{fl} \times \lvert g_{lum}\rvert$.

pentahelicene).[80] In contrast to the pentahelicenes, heating an enantiopure sample of hexahelicene **BN[6]** to 200 °C for 14 h did not induce any racemization as analyzed by (CSP)-HPLC. Instead, higher temperatures caused a rapid decomposition.

In order to understand the influence of BN- and mesityl-substitution on the racemization, we calculated the respective transition states and activation barriers (see ESI, Section 7.2†). Although the absolute theoretical values of $\Delta G^{\ddagger}$ (T) were higher than the experimental ones, a gain in configurational stability upon BN-substitution was reproduced. We attribute this to the dipolar repulsions of the opposite NH hydrogen atoms, which are in significantly closer proximity in the transition state ($d \approx$ 1.5 Å for **BN[5]**) than in the C_2-symmetric ground state ($d = 2.2$ Å in a crystal). In contrast, the parallelly aligned but distant mesityl groups in the transition states do not appear to play a major role.

Chiroptical spectroscopy

Electronic Circular Dichroism (ECD) measurements of the highly enriched enantiomers throughout resulted in mirror-imaged spectra (Fig. 4 and Table 2).

In all cases, the correlation with the computed rotatory strengths R_{vel} allowed us to assign that the absolute configuration of the first fraction from (CSP)-HPLC was (*P*), which corresponds to parent penta- and hexahelicenes (Fig. 4).[69]

The (*P*)-enantiomers of **BN[5]** (λ = 393 nm, $\Delta\varepsilon$ = +111 M^{-1} cm^{-1}) and **BN[5]-(CN)$_2$** (λ = 412 nm, $\Delta\varepsilon$ = +127 M^{-1} cm^{-1}) revealed intense, positive Cotton effects (CE) in the low-energy region. Comparably sharp, negative CE maxima were located at $\lambda \approx 300$ nm. In contrast, the band that represents the ^1L_a transition of (*P*)-**CC[5]** (λ = 399 nm, $\Delta\varepsilon$ = −1.8 M^{-1} cm^{-1}) was barely visible (Fig. 4b), which closely resembles the parent pentahelicene.[22] Moreover, the band for the ^1B_b transition was mirrored as a positive CE at $\lambda = 319$ nm ($\Delta\varepsilon$ = +152 M^{-1} cm^{-1}).

The ECD spectra of (*P*)-**BN[6]** and (mono)BN-hexahelicene (Fig. 1, top right)[50] were similarly shaped, with one strongly negative CE ($\lambda = 285$ nm, $\Delta\varepsilon = -151$ M^{-1} cm^{-1} for **BN[6]**, λ = 245 nm, $\Delta\varepsilon = -290$ M^{-1} cm^{-1} for the reported compound) and several less intense CE with opposite sign at higher wavelengths. As for the absorption and emission maxima, a twofold BN-substitution induced a significant bathochromic shift of the whole ECD spectrum ($\Delta\lambda \approx 40$ nm).

The experimental absorption dissymmetry factors were typical of helicenes ($|g_{abs}| = 6$–11×10^{-3}, *cf.* 7.6×10^{-3} for pentahelicene[22] and 9.2×10^{-3} for hexahelicene,[23] in DCM solutions at 25 °C, see ESI, Section 5.4†). By means of TD-DFT calculations, we analyzed the contributions of electric ($|\mu|$) and magnetic ($|m|$) transition dipole moments and the angle between both (θ) on absorption dissymmetries. For helicenes, the simplified expression $g_{abs} \approx 4 \times |m| \times \cos(\theta)/|\mu|$ applies.[81] Due to the good reproduction of the experimental transition energies, we made use of the same level of theory as applied previously, although several recent studies reveal the accurate prediction of $|g_{abs}|$ and $|g_{lum}|$ values by using long-range corrected functionals (see ESI, Section 7.7†).[82–84]

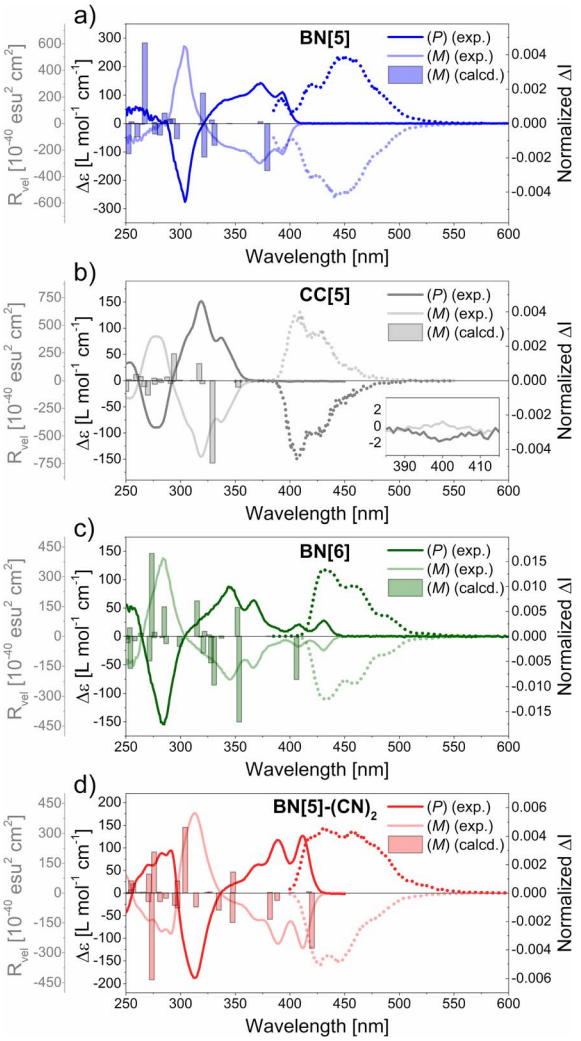

Fig. 4 Experimental ECD (continuous lines) and CPL (dotted lines) spectra in DCM ($c = 1.3 \times 10^{-5}$ to 4.0×10^{-5} M) as well as computed rotatory strengths (bars outlined in grey). ΔI was normalized to the respective global maxima of $|g_{lum}|$.

For **BN[5]** and **BN[5]-(CN)$_2$**, strongly enhanced transition dipole moments (≈ thirtyfold increases of |m| and ≈ tenfold increases of |μ|), compared to **CC[5]**), were calculated for the lowest-energy transitions (see ESI, Tables S55 and S56†). However, the favorable, parallel orientations of the transition dipole moments of **CC[5]** ($\theta = 0°$, *cf.* 114° for **BN[5]**) balanced out the BN-induced increase of |m|, so that $|g_{abs}| \approx 1.0–1.3 \times 10^{-2}$ for all pentahelicenes. With respect to the $S_0 \rightarrow S_1$ transitions of the hexahelicenes, both |μ| and |m| of **BN[6]** were enhanced only by a factor of four, compared to **CC[6]**. Here, the more favorably aligned dipole moments result in a considerably enhanced theoretical absorption dissymmetry.

TD-DFT calculations of the geometry-optimized structures in the S_1 states also allowed us to obtain the theoretical luminescence dissymmetry factors $|g_{lum}|$ (see ESI, Table S56†). Overall, the absolute values of |μ|, |m| and θ of the $S_1 \rightarrow S_0$ transition were comparable with the $S_0 \rightarrow S_1$ transition, so that $|g_{lum}| = 0.74–1.02 \times |g_{abs}|$. Although the calculated bond lengths were very similar in both electronic states, the disparities in plane-to-plane angles were more pronounced, leading to deviating geometries (see ESI, Tables S49–53†).

Despite the previously discussed small Stokes shifts (Table 1), this could contribute to the experimental and theoretical differences between $|g_{abs}|$ and $|g_{lum}|$.

Experimental CPL spectra were obtained and normalized to the respective maxima of g_{lum} (Fig. 4 and ESI, Section 5.5†). In all cases, the sign of the CPL was identical with the sign of the lowest-energy transition in ECD. All pentahelicenes revealed comparable luminescence dissymmetry factors ($|g_{lum}| = 4–5 \times 10^{-3}$), which is in good agreement with the empirically observed correlation in helicenes ($g_{lum} \approx 0.61 \times g_{abs}$) in the case of **CC[5]** and **BN[5]-(CN)$_2$**.[85] Due to the enhanced fluorescence quantum yields of both BN-pentahelicenes, their CPL brightness factors were considerably elevated ($B_{CPL} > 10$ M^{-1} cm^{-1}) compared to **CC[5]** ($B_{CPL} = 3.0$ M^{-1} cm^{-1}).

BN[6] exhibited an outstanding experimental value of $|g_{lum}| = 1.33 \times 10^{-2}$, which is considerably higher than of unsubstituted hexahelicene ($|g_{lum}| = 9 \times 10^{-4}$).[23] In accordance with that, the theoretical values ($|g_{lum}| = 2.3 \times 10^{-2}$ for **BN[6]**, $|g_{lum}| = 0.6 \times 10^{-2}$ for **CC[6]**) indicate a stronger impact of BN-substitution on a hexahelicene than on a pentahelicene. In particular, the much more favorable orientation of the transition dipole moments in **BN[6]** (135°, *cf.* 102° for **CC[6]**) is the most significant contributor to the dramatically improved theoretical $|g_{lum}|$ value.

Compared to several reported helicenes[84,86] with coordinative B←N-bonds ($|g_{lum}| = 0.25–3.5 \times 10^{-3}$ and $B_{CPL} < 10$ M^{-1} cm^{-1}), the combination of increased φ_{fl} and $|g_{lum}|$ values led to a CPL brightness of $B_{CPL} = 59$ M^{-1} cm^{-1} for **BN[6]**. This value is exceptionally high for a non-π-extended, monomeric helicene, and proves that BN-doping of helicenes is a concept that could foster the development of potent CPL emitting materials.

Conclusions

In summary, we have prepared and investigated the first examples of fully conjugated and non-π-extended (bis)BN-substituted penta- and hexahelicenes. Comparing them with their all-carbon congeners allowed the precise estimation of the influence of such BN-doping.

As seen from the solid-state structures, the helix torsion of pentahelicene **BN[5]** was significantly smaller than of **CC[5]**. Owing to a larger spatial separation, this was not the case for **BN[6]**, resulting in congruent structures of both hexahelicenes. The impact of BN-substitution on λ_{abs} and λ_{fl} was rather small ($\Delta\lambda \approx 10–15$ nm). However, both the intensities of the low-energy absorptions as well as the φ_{fl} values were significantly elevated, peaking at 0.17 (**BN[6]**) and 0.25 (**BN[5]-(CN)$_2$**). TD-DFT calculations allowed us to reproduce the causal, largely increased oscillator strengths of the BN-helicenes, being attributable to the reduction of symmetry. With respect to the configurational stabilities, **BN[5]** ($t_{1/2rac} \approx 80$ min at 60 °C) racemized four times slower than **CC[5]**, which is possibly due to NH-repulsions in the transition state.

Mirror-imaged ECD spectra were obtained and, according to the strengthened low-energy absorptions, the $\Delta\varepsilon$ was considerably intensified in this region for the BN-pentahelicenes, as well. Regarding CPL, the $|g_{lum}|$ value of **BN[6]** (1.33×10^{-2}, *cf.* hexahelicene: 9×10^{-4}) was unusually high, as elevated dissymmetry factors are usually associated with a loss of fluorescence efficiency.[13]

Taking into account that a selective dibromination of **BN[5]** was possible and the boron atoms may be modified with nucleophilic groups at an earlier stage of the reaction sequence,[87] BN-helicenes with tailored push–pull substitution patterns could be synthesized in the future in order to explore their potential as efficient CPL emitters.

Data availability

Experimental and theoretical details supporting the statements of this article are included in the ESI.†

Author contributions

Y. A. and A. S. conceived the project. Y. A. and N. W. performed the syntheses and routine analytics. Y. A. and S. M. L. performed the chiral resolutions, kinetics and chiroptical measurements, which were supervised by A. G. C. and M. J. P. P. performed the X-ray diffraction analyses. Y. A., S. M. L. and S. K. performed the DFT calculations, which were supervised by T. N. M. M. collected the quantum yields. D. M. performed the lifetime and excitation experiments. The manuscript was written by Y. A and S. M. L. All authors participated in reviewing the manuscript.

Conflicts of interest

There are no conflicts to declare.

Acknowledgements

A.G.C. and S.M.L. acknowledge grant PID2021-127521NB-I00 funded by MCIN/AEI/10.13039/501100011033, the European Regional Development Fund (ERDF) "A way of making Europe" and Ministerio de Economía y Competitividad (BES-2016-076371). S.M.L. acknowledges the Spanish Junta de Andalucía for funding. P.P. acknowledges the Central Research Development Fund of the University of Bremen for the postdoctoral fellowship. M.J. acknowledges the European Research Council (ERC) under the European Union's Horizon 2020 research and innovation programme (grant agreement no. 716139) and the Swiss National Science Foundation (SNSF; no. PP00P2_198900). We thank Prof. A. J. Mota from the Department of Inorganic Chemistry from the University of Granada for performing additional DFT calculations.

Notes and references

1 J. Crassous, in *Circularly Polarized Luminescence of Isolated Small Organic Molecules*, ed. T. Mori, Springer Singapore, Singapore, 2020, pp. 53–97.
2 Y. Yang, R. C. da Costa, M. J. Fuchter and A. J. Campbell, Circularly polarized light detection by a chiral organic semiconductor transistor, *Nat. Photonics*, 2013, **7**, 634–638.
3 M. Li, S.-H. Li, D. Zhang, M. Cai, L. Duan, M.-K. Fung and C.-F. Chen, Stable Enantiomers Displaying Thermally Activated Delayed Fluorescence: Efficient OLEDs with Circularly Polarized Electroluminescence, *Angew. Chem., Int. Ed.*, 2018, **57**, 2889–2893.
4 J. Crassous, M. J. Fuchter, D. E. Freedman, N. A. Kotov, J. Moon, M. C. Beard and S. Feldmann, Materials for chiral light control, *Nat. Rev. Mater.*, 2023, **8**, 365–371.
5 M. Schadt, Liquid Crystal Materials and Liquid Crystal Displays, *Annu. Rev. Mater. Sci.*, 1997, **27**, 305–379.
6 Y. Yang, R. C. da Costa, D.-M. Smilgies, A. J. Campbell and M. J. Fuchter, Induction of Circularly Polarized Electroluminescence from an Achiral Light-Emitting Polymer via a Chiral Small-Molecule Dopant, *Adv. Mater.*, 2013, **25**, 2624–2628.
7 N. P. M. Huck, W. F. Jager, B. de Lange and B. L. Feringa, Dynamic Control and Amplification of Molecular Chirality by Circular Polarized Light, *Science*, 1996, **273**, 1686–1688.
8 M. Suarez and G. B. Schuster, Photoresolution of an Axially Chiral Bicyclo[3.3.0]octan-3-one: Phototriggers for a Liquid-Crystal-Based Optical Switch, *J. Am. Chem. Soc.*, 1995, **117**, 6732–6738.
9 N. Nishizawa and H. Munekata, Lateral-Type Spin-Photonics Devices: Development and Applications, *Micromachines*, 2021, **12**, 644.
10 R. Farshchi, M. Ramsteiner, J. Herfort, A. Tahraoui and H. T. Grahn, Optical communication of spin information between light emitting diodes, *Appl. Phys. Lett.*, 2011, **98**, 162508.
11 G. Muller, Luminescent chiral lanthanide(iii) complexes as potential molecular probes, *Dalton Trans.*, 2009, 9692–9707.
12 C. P. Montgomery, E. J. New, D. Parker and R. D. Peacock, Enantioselective regulation of a metal complex in reversible binding to serum albumin: dynamic helicity inversion signalled by circularly polarised luminescence, *Chem. Commun.*, 2008, **36**, 4261–4263.
13 E. M. Sánchez-Carnerero, A. R. Agarrabeitia, F. Moreno, B. L. Maroto, G. Muller, M. J. Ortiz and S. de la Moya, Circularly Polarized Luminescence from Simple Organic Molecules, *Chem.–Euro. J.*, 2015, **21**, 13488–13500.
14 D.-Q. He, H.-Y. Lu, M. Li and C.-F. Chen, Intense blue circularly polarized luminescence from helical aromatic esters, *Chem. Commun.*, 2017, **53**, 6093–6096.
15 X.-F. Luo, H.-B. Han, Z.-P. Yan, Z.-G. Wu, J. Su, J.-W. Zou, Z.-Q. Zhu, Y.-X. Zheng and J.-L. Zuo, Multicolor Circularly Polarized Photoluminescence and Electroluminescence with 1,2-Diaminecyclohexane Enantiomers, *ACS Appl. Mater. Interfaces*, 2020, **12**, 23172–23180.
16 M. Gingras, One hundred years of helicene chemistry. Part 1: non-stereoselective syntheses of carbohelicenes, *Chem. Soc. Rev.*, 2013, **42**, 968–1006.
17 J. Crassous, I. G. Stará and I. Stary, *Helicenes: Synthesis, Properties and Applications*, Wiley-VCH, Weinheim, 2022.

18 P. Ravat, R. Hinkelmann, D. Steinebrunner, A. Prescimone, I. Bodoky and M. Juríček, Configurational Stability of [5] Helicenes, *Org. Lett.*, 2017, **19**, 3707–3710.
19 Y. Shen and C.-F. Chen, Helicenes: Synthesis and Applications, *Chem. Rev.*, 2012, **112**, 1463–1535.
20 L. Arrico, L. Di Bari and F. Zinna, Quantifying the Overall Efficiency of Circularly Polarized Emitters, *Chem.–Euro. J.*, 2021, **27**, 2920–2934.
21 M. Sapir and E. V. Donckt, Intersystem crossing in the helicenes, *Chem. Phys. Lett.*, 1975, **36**, 108–110.
22 H. Tanaka, Y. Kato, M. Fujiki, Y. Inoue and T. Mori, Combined Experimental and Theoretical Study on Circular Dichroism and Circularly Polarized Luminescence of Configurationally Robust D3-Symmetric Triple Pentahelicene, *J. Phys. Chem. A*, 2018, **122**, 7378–7384.
23 H. Tanaka, M. Ikenosako, Y. Kato, M. Fujiki, Y. Inoue and T. Mori, Symmetry-based rational design for boosting chiroptical responses, *Commun. Chem.*, 2018, **1**, 38.
24 D. Göbel, S. Míguez-Lago, M. J. Ruedas-Rama, A. Orte, A. G. Campaña and M. Juríček, Circularly Polarized Luminescence of [6]Helicenes through Excited-State Intramolecular Proton Transfer, *Helv. Chim. Acta*, 2022, **105**, e202100221.
25 F. Chen, T. Tanaka, T. Mori and A. Osuka, Synthesis, Structures, and Optical Properties of Azahelicene Derivatives and Unexpected Formation of Azahepta[8] circulates, *Chem.–Euro. J.*, 2018, **24**, 7489–7497.
26 T. Otani, A. Tsuyuki, T. Iwachi, S. Someya, K. Tateno, H. Kawai, T. Saito, K. S. Kanyiva and T. Shibata, Facile Two-Step Synthesis of 1,10-Phenanthroline-Derived Polyaza [7]helicenes with High Fluorescence and CPL Efficiency, *Angew. Chem., Int. Ed.*, 2017, **56**, 3906–3910.
27 K. Goto, R. Yamaguchi, S. Hiroto, H. Ueno, T. Kawai and H. Shinokubo, Intermolecular Oxidative Annulation of 2-Aminoanthracenes to Diazaacenes and Aza[7]helicenes, *Angew. Chem., Int. Ed.*, 2012, **51**, 10333–10336.
28 H. Nishimura, K. Tanaka, Y. Morisaki, Y. Chujo, A. Wakamiya and Y. Murata, Oxygen-Bridged Diphenylnaphthylamine as a Scaffold for Full-Color Circularly Polarized Luminescent Materials, *J. Org. Chem.*, 2017, **82**, 5242–5249.
29 T. Matsuno, Y. Koyama, S. Hiroto, J. Kumar, T. Kawai and H. Shinokubo, Isolation of a 1,4-diketone intermediate in oxidative dimerization of 2-hydroxyanthracene and its conversion to oxahelicene, *Chem. Commun.*, 2015, **51**, 4607–4610.
30 M. Murai, R. Okada, A. Nishiyama and K. Takai, Synthesis and Properties of Sila[n]helicenes via Dehydrogenative Silylation of C–H Bonds under Rhodium Catalysis, *Org. Lett.*, 2016, **18**, 4380–4383.
31 H. Oyama, K. Nakano, T. Harada, R. Kuroda, M. Naito, K. Nobusawa and K. Nozaki, Facile Synthetic Route to Highly Luminescent Sila[7]helicene, *Org. Lett.*, 2013, **15**, 2104–2107.
32 T. Katayama, S. Nakatsuka, H. Hirai, N. Yasuda, J. Kumar, T. Kawai and T. Hatakeyama, Two-Step Synthesis of Boron-Fused Double Helicenes, *J. Am. Chem. Soc.*, 2016, **138**, 5210–5213.
33 K. Dhbaibi, L. Favereau and J. Crassous, Enantioenriched Helicenes and Helicenoids Containing Main-Group Elements (B, Si, N, P), *Chem. Rev.*, 2019, **119**, 8846–8953.
34 *Formal charges at the B=N groups omitted because the aromaticity of the 1,2-azaborinine rings was verified both experimentally and theoretically*.
35 A. Abengózar, P. García-García, M. A. Fernández-Rodríguez, D. Sucunza and J. J. Vaquero, in *Advances in Heterocyclic Chemistry*, ed. E. F. V. Scriven and C. A. Ramsden, Academic Press, 2021, vol. 135, pp. 197–259.
36 J. Hoffmann, B. Geffroy, E. Jaques, M. Hissler and A. Staubitz, Tuning the aggregation behaviour of BN-coronene diimides with imide substituents and their performance in devices (OLEDs and OFETs), *J. Mater. Chem. C*, 2021, **9**, 14720–14729.
37 J. Hoffmann, D. Jacquemin, M. Hissler and A. Staubitz, BN-Substituted Coronene Diimide Donor–Acceptor–Donor Triads: Photophysical, (Spectro)-Electrochemical Studies and Lewis Behavior, *J. Mater. Chem. C*, 2021, **9**, 13926–13934.
38 L. Palomino-Ruiz, S. Rodríguez-González, J. G. Fallaque, I. R. Márquez, N. Agraït, C. Díaz, E. Leary, J. M. Cuerva, A. G. Campaña, F. Martín, A. Millán and M. T. González, Single-Molecule Conductance of 1,4-Azaborine Derivatives as Models of BN-doped PAHs, *Angew. Chem., Int. Ed.*, 2021, **60**, 6609–6616.
39 Y. Appiarius and A. Staubitz, Azaborinine, *Chem. Unserer Zeit*, 2023, **57**, 180–190.
40 S. Hashimoto, T. Ikuta, K. Shiren, S. Nakatsuka, J. Ni, M. Nakamura and T. Hatakeyama, Triplet-Energy Control of Polycyclic Aromatic Hydrocarbons by BN Replacement: Development of Ambipolar Host Materials for Phosphorescent Organic Light-Emitting Diodes, *Chem. Mater.*, 2014, **26**, 6265–6271.
41 J. S. A. Ishibashi, J. L. Marshall, A. Mazière, G. J. Lovinger, B. Li, L. N. Zakharov, A. Dargelos, A. Graciaa, A. Chrostowska and S.-Y. Liu, Two BN Isosteres of Anthracene: Synthesis and Characterization, *J. Am. Chem. Soc.*, 2014, **136**, 15414–15421.
42 Y. Appiarius, P. J. Gliese, S. A. W. Segler, P. Rusch, J. Zhang, P. J. Gates, R. Pal, L. A. Malaspina, K. Sugimoto, T. Neudecker, N. C. Bigall, S. Grabowsky, A. A. Bakulin and A. Staubitz, BN-Substitution in Dithienylpyrenes Prevents Excimer Formation in Solution and in the Solid State, *J. Phys. Chem. C*, 2022, **126**, 4563–4576.
43 J. Full, S. P. Panchal, J. Götz, A.-M. Krause and A. Nowak-Król, Modular Synthesis of Organoboron Helically Chiral Compounds: Cutouts from Extended Helices, *Angew. Chem., Int. Ed.*, 2021, **60**, 4350–4357.
44 J.-K. Li, X.-Y. Chen, Y.-L. Guo, X.-C. Wang, A. C. H. Sue, X.-Y. Cao and X.-Y. Wang, B,N-Embedded Double Hetero[7] helicenes with Strong Chiroptical Responses in the Visible Light Region, *J. Am. Chem. Soc.*, 2021, **143**, 17958–17963.
45 F. Full, Q. Wölflick, K. Radacki, H. Braunschweig and A. Nowak-Król, Enhanced Optical Properties of Azaborole

Helicenes by Lateral and Helical Extension, *Chem.–Euro. J.*, 2022, **28**, e202202280.

46 J. Guo, Z. Li, X. Tian, T. Zhang, Y. Wang and C. Dou, Diradical B/N-Doped Polycyclic Hydrocarbons, *Angew. Chem., Int. Ed.*, 2023, **62**, e202217470.

47 F. Zhang, F. Rauch, A. Swain, T. B. Marder and P. Ravat, Efficient Narrowband Circularly Polarized Light Emitters Based on 1,4-B,N-embedded Rigid Donor–Acceptor Helicenes, *Angew. Chem., Int. Ed.*, 2023, **62**, e202218965.

48 T. Hatakeyama, S. Hashimoto, T. Oba and M. Nakamura, Azaboradibenzo[6]helicene: Carrier Inversion Induced by Helical Homochirality, *J. Am. Chem. Soc.*, 2012, **134**, 19600–19603.

49 A. Abengózar, P. García-García, D. Sucunza, A. Pérez-Redondo and J. J. Vaquero, Synthesis of functionalized helical BN-benzo[c]phenanthrenes, *Chem. Commun.*, 2018, **54**, 2467–2470.

50 K. Yuan, D. Volland, S. Kirschner, M. Uzelac, G. S. Nichol, A. Nowak-Król and M. J. Ingleson, Enhanced N-directed electrophilic C–H borylation generates BN–[5]- and [6] helicenes with improved photophysical properties, *Chem. Sci.*, 2022, **13**, 1136–1145.

51 M. Buchta, J. Rybáček, A. Jančařík, A. A. Kudale, M. Buděšínský, J. V. Chocholoušová, J. Vacek, L. Bednárová, I. Císařová, G. J. Bodwell, I. Starý and I. G. Stará, Chimerical Pyrene-Based [7]Helicenes as Twisted Polycondensed Aromatics, *Chem.–Euro. J.*, 2015, **21**, 8910–8917.

52 L. D. M. Nicholls, M. Marx, T. Hartung, E. González-Fernández, C. Golz and M. Alcarazo, TADDOL-Derived Cationic Phosphonites: Toward an Effective Enantioselective Synthesis of [6]Helicenes via Au-Catalyzed Alkyne Hydroarylation, *ACS Catal.*, 2018, **8**, 6079–6085.

53 A. Jančařík, J. Rybáček, K. Cocq, J. Vacek Chocholoušová, J. Vacek, R. Pohl, L. Bednárová, P. Fiedler, I. Císařová, I. G. Stará and I. Starý, Rapid Access to Dibenzohelicenes and their Functionalized Derivatives, *Angew. Chem., Int. Ed.*, 2013, **52**, 9970–9975.

54 A. W. Baggett, M. Vasiliu, B. Li, D. A. Dixon and S.-Y. Liu, Late-Stage Functionalization of 1,2-Dihydro-1,2-azaborines via Regioselective Iridium-Catalyzed C–H Borylation: The Development of a New N,N-Bidentate Ligand Scaffold, *J. Am. Chem. Soc.*, 2015, **137**, 5536–5541.

55 Y. Appiarius, T. Stauch, E. Lork, P. Rusch, N. C. Bigall and A. Staubitz, From a 1,2-Azaborinine to Large BN-PAHs via Electrophilic Cyclization: Synthesis, Characterization and Promising Optical Properties, *Org. Chem. Front.*, 2021, **8**, 10–17.

56 S. Eissler, M. Kley, D. Bächle, G. Loidl, T. Meier and D. Samson, Substitution determination of Fmoc-substituted resins at different wavelengths, *J. Pept. Sci.*, 2017, **23**, 757–762.

57 C. A. Merlic and M. E. Pauly, Ruthenium-Catalyzed Cyclizations of Dienylalkynes Via Vinylidene Intermediates, *J. Am. Chem. Soc.*, 1996, **118**, 11319–11320.

58 C. R. McConnell and S.-Y. Liu, Late-stage functionalization of BN-heterocycles, *Chem. Soc. Rev.*, 2019, **48**, 3436–3453.

59 L. Zi, J. Zhang, C. Li, Y. Qu, B. Zhen, X. Liu and L. Zhang, Synthesis, Properties, and Reactivity of Bis-BN Phenanthrenes: Stepwise Bromination of the Main Scaffold, *Org. Lett.*, 2020, **22**, 1499–1503.

60 A. Abengózar, I. Valencia, G. G. Otárola, D. Sucunza, P. García-García, A. Pérez-Redondo, F. Mendicuti and J. J. Vaquero, Expanding the BN-embedded PAH family: 4a-aza-12a-borachrysene, *Chem. Commun.*, 2020, **56**, 3669–3672.

61 C. Zhang, BN-Phenanthrenes: Synthesis, Reactivity, and Optical Properties, *Org. Lett.*, 2019, **21**, 3476–3480.

62 M. Solà, Forty years of Clar's aromatic π-sextet rule, *Front. Chem.*, 2013, **1**, 22.

63 P. G. Campbell, A. J. V. Marwitz and S.-Y. Liu, Recent Advances in Azaborine Chemistry, *Angew. Chem., Int. Ed.*, 2012, **51**, 6074–6092.

64 M. J. Frisch, M. Head-Gordon and J. A. Pople, A direct MP2 gradient method, *Chem. Phys. Lett.*, 1990, **166**, 275–280.

65 T. H. Dunning Jr, Gaussian Basis Sets for Use in Correlated Molecular Calculations. I. The Atoms Boron Through Neon and Hydrogen, *J. Chem. Phys.*, 1989, **90**, 1007–1023.

66 E. Epifanovsky, A. T. B. Gilbert, X. Feng, J. Lee, Y. Mao, N. Mardirossian, P. Pokhilko, A. F. White, M. P. Coons, A. L. Dempwolff, Z. Gan, D. Hait, P. R. Horn, L. D. Jacobson, I. Kaliman, J. Kussmann, A. W. Lange, K. U. Lao, D. S. Levine, J. Liu, S. C. McKenzie, A. F. Morrison, K. D. Nanda, F. Plasser, D. R. Rehn, M. L. Vidal, Z.-Q. You, Y. Zhu, B. Alam, B. J. Albrecht, A. Aldossary, E. Alguire, J. H. Andersen, V. Athavale, D. Barton, K. Begam, A. Behn, N. Bellonzi, Y. A. Bernard, E. J. Berquist, H. G. A. Burton, A. Carreras, K. Carter-Fenk, R. Chakraborty, A. D. Chien, K. D. Closser, V. Cofer-Shabica, S. Dasgupta, M. de Wergifosse, J. Deng, M. Diedenhofen, H. Do, S. Ehlert, P.-T. Fang, S. Fatehi, Q. Feng, T. Friedhoff, J. Gayvert, Q. Ge, G. Gidofalvi, M. Goldey, J. Gomes, C. E. González-Espinoza, S. Gulania, A. O. Gunina, M. W. D. Hanson-Heine, P. H. P. Harbach, A. Hauser, M. F. Herbst, M. Hernández Vera, M. Hodecker, Z. C. Holden, S. Houck, X. Huang, K. Hui, B. C. Huynh, M. Ivanov, Á. Jász, H. Ji, H. Jiang, B. Kaduk, S. Kähler, K. Khistyaev, J. Kim, G. Kis, P. Klunzinger, Z. Koczor-Benda, J. H. Koh, D. Kosenkov, L. Koulias, T. Kowalczyk, C. M. Krauter, K. Kue, A. Kunitsa, T. Kus, I. Ladjánszki, A. Landau, K. V. Lawler, D. Lefrancois, S. Lehtola, R. R. Li, Y.-P. Li, J. Liang, M. Liebenthal, H.-H. Lin, Y.-S. Lin, F. Liu, K.-Y. Liu, M. Loipersberger, A. Luenser, A. Manjanath, P. Manohar, E. Mansoor, S. F. Manzer, S.-P. Mao, A. V. Marenich, T. Markovich, S. Mason, S. A. Maurer, P. F. McLaughlin, M. F. S. J. Menger, J.-M. Mewes, S. A. Mewes, P. Morgante, J. W. Mullinax, K. J. Oosterbaan, G. Paran, A. C. Paul, S. K. Paul, F. Pavošević, Z. Pei, S. Prager, E. I. Proynov, Á. R. ák, E. Ramos-Cordoba, B. Rana, A. E. Rask, A. Rettig, R. M. Richard, F. Rob, E. Rossomme, T. Scheele, M. Scheurer, M. Schneider, N. Sergueev, S. M. Sharada, W. Skomorowski, D. W. Small, C. J. Stein, Y.-C. Su, E. J. Sundstrom, Z. Tao, J. Thirman, G. J. Tornai, T. Tsuchimochi, N. M. Tubman, S. P. Veccham, O. Vydrov, J. Wenzel, J. Witte, A. Yamada,

K. Yao, S. Yeganeh, S. R. Yost, A. Zech, I. Y. Zhang, X. Zhang, Y. Zhang, D. Zuev, A. Aspuru-Guzik, A. T. Bell, N. A. Besley, K. B. Bravaya, B. R. Brooks, D. Casanova, J.-D. Chai, S. Coriani, C. J. Cramer, G. Cserey, A. E. DePrince III, R. A. DiStasio Jr, A. Dreuw, B. D. Dunietz, T. R. Furlani, W. A. Goddard III, S. Hammes-Schiffer, T. Head-Gordon, W. J. Hehre, C.-P. Hsu, T.-C. Jagau, Y. Jung, A. Klamt, J. Kong, D. S. Lambrecht, W. Liang, N. J. Mayhall, C. W. McCurdy, J. B. Neaton, C. Ochsenfeld, J. A. Parkhill, R. Peverati, V. A. Rassolov, Y. Shao, L. V. Slipchenko, T. Stauch, R. P. Steele, J. E. Subotnik, A. J. W. Thom, A. Tkatchenko, D. G. Truhlar, T. Van Voorhis, T. A. Wesolowski, K. B. Whaley, H. L. Woodcock III, P. M. Zimmerman, S. Faraji, P. M. W. Gill, M. Head-Gordon, J. M. Herbert and A. I. Krylov, Software for the frontiers of quantum chemistry: An overview of developments in the Q-Chem 5 package, *J. Chem. Phys.*, 2021, 155.

67 Z. Chen, C. S. Wannere, C. Corminboeuf, R. Puchta and P. V. R. Schleyer, Nucleus-Independent Chemical Shifts (NICS) as an Aromaticity Criterion, *Chem. Rev.*, 2005, **105**, 3842–3888.

68 T. Mori, Chiroptical Properties of Symmetric Double, Triple, and Multiple Helicenes, *Chem. Rev.*, 2021, **121**, 2373–2412.

69 F. Furche, R. Ahlrichs, C. Wachsmann, E. Weber, A. Sobanski, F. Vögtle and S. Grimme, Circular Dichroism of Helicenes Investigated by Time-Dependent Density Functional Theory, *J. Am. Chem. Soc.*, 2000, **122**, 1717–1724.

70 Y. Nakai, T. Mori, K. Sato and Y. Inoue, Theoretical and Experimental Studies of Circular Dichroism of Mono- and Diazonia[6]helicenes, *J. Phys. Chem. A*, 2013, **117**, 5082–5092.

71 J. B. Birks, D. J. S. Birch, E. Cordemans and E. Vander Donckt, Fluorescence of the higher helicenes, *Chem. Phys. Lett.*, 1976, **43**, 33–36.

72 A. J. V. Marwitz, M. H. Matus, L. N. Zakharov, D. A. Dixon and S.-Y. Liu, A Hybrid Organic/Inorganic Benzene, *Angew. Chem., Int. Ed.*, 2009, **48**, 973–977.

73 A. D. Becke, Density-Functional Exchange-Energy Approximation with Correct Asymptotic Behavior, *Phys. Rev. A*, 1988, **38**, 3098–3100.

74 A. D. Becke, A New Mixing of Hartree–Fock and Local Density-Functional Theories, *J. Chem. Phys.*, 1993, **98**, 1372–1377.

75 C. Lee, W. Yang and R. G. Parr, Development of the Colle-Salvetti Correlation-Energy Formula into a Functional of the Electron Density, *Phys. Rev. B*, 1988, **37**, 785–789.

76 H. Kubo, T. Hirose and K. Matsuda, Control over the Emission Properties of [5]Helicenes Based on the Symmetry and Energy Levels of Their Molecular Orbitals, *Org. Lett.*, 2017, **19**, 1776–1779.

77 M. J. Frisch, G. W. Trucks, H. B. Schlegel, G. E. Scuseria, M. A. Robb, J. R. Cheeseman, G. Scalmani, V. Barone, B. Mennucci, G. A. Petersson, H. Nakatsuji, M. Caricato, X. Li, H. P. Hratchian, A. F. Izmaylov, J. Bloino, G. Zheng, J. L. Sonnenberg, M. Hada, M. Ehara, K. Toyota, R. Fukuda, J. Hasegawa, M. Ishida, T. Nakajima, Y. Honda, O. Kitao, H. Nakai, T. Vreven, J. A. Montgomery, J. E. Peralta, F. Ogliaro, M. Bearpark, J. J. Heyd, E. Brothers, K. N. Kudin, V. N. Staroverov, R. Kobayashi, J. Normand, K. Raghavachari, A. Rendell, J. C. Burant, S. S. Iyengar, J. Tomasi, M. Cossi, N. Rega, J. M. Millam, M. Klene, J. E. Knox, J. B. Cross, V. Bakken, C. Adamo, J. Jaramillo, R. Gomperts, R. E. Stratmann, O. Yazyev, A. J. Austin, R. Cammi, C. Pomelli, J. W. Ochterski, R. L. Martin, K. Morokuma, V. G. Zakrzewski, G. A. Voth, P. Salvador, J. J. Dannenberg, S. Dapprich, A. D. Daniels, Ö. Farkas, J. B. Foresman, J. V. Ortiz, J. Cioslowski and D. J. Fox, *Gaussian 09, Rev. B.01*, Wallingford CT, 2010.

78 M. Kasha, Characterization of electronic transitions in complex molecules, *Discuss. Faraday Soc.*, 1950, **9**, 14–19.

79 H. Görner, C. Stammel and J. Mattay, Excited state behaviour of pentahelicene dinitriles, *J. Photochem. Photobiol., A*, 1999, **120**, 171–179.

80 P. Ravat, Carbo[n]helicenes Restricted to Enantiomerize: An Insight into the Design Process of Configurationally Stable Functional Chiral PAHs, *Chem.–Euro. J.*, 2021, **27**, 3957–3967.

81 M. Cei, L. Di Bari and F. Zinna, Circularly polarized luminescence of helicenes: A data-informed insight, *Chirality*, 2023, **35**, 192–210.

82 C. A. Guido, F. Zinna and G. Pescitelli, CPL calculations of [7]helicenes with alleged exceptional emission dissymmetry values, *J. Mater. Chem. C*, 2023, **11**, 10474–10482.

83 K. Dhbaibi, L. Abella, S. Meunier-Della-Gatta, T. Roisnel, N. Vanthuyne, B. Jamoussi, G. Pieters, B. Racine, E. Quesnel, J. Autschbach, J. Crassous and L. Favereau, Achieving high circularly polarized luminescence with push–pull helicenic systems: from rationalized design to top-emission CP-OLED applications, *Chem. Sci.*, 2021, **12**, 5522–5533.

84 Z. Domínguez, R. López-Rodríguez, E. Álvarez, S. Abbate, G. Longhi, U. Pischel and A. Ros, Azabora[5]helicene Charge-Transfer Dyes Show Efficient and Spectrally Variable Circularly Polarized Luminescence, *Chem.–Euro. J.*, 2018, **24**, 12660–12668.

85 H. Tanaka, Y. Inoue and T. Mori, Circularly Polarized Luminescence and Circular Dichroisms in Small Organic Molecules: Correlation between Excitation and Emission Dissymmetry Factors, *ChemPhotoChem*, 2018, **2**, 386–402.

86 C. Shen, M. Srebro-Hooper, M. Jean, N. Vanthuyne, L. Toupet, J. A. G. Williams, A. R. Torres, A. J. Riives, G. Muller, J. Autschbach and J. Crassous, Synthesis and Chiroptical Properties of Hexa-, Octa-, and Deca-azaborahelicenes: Influence of Helicene Size and of the Number of Boron Atoms, *Chem.–Euro. J.*, 2017, **23**, 407–418.

87 A. W. Baggett and S.-Y. Liu, A Boron Protecting Group Strategy for 1,2-Azaborines, *J. Am. Chem. Soc.*, 2017, **139**, 15259–15264.